Turbulent drag reduction by wavy wall

Sacha Ghebali

Department of Aeronautics
Imperial College London
Exhibition road, London SW7 2AZ, UK
s.ghebali14@imperial.ac.uk

Sergei Chernyshenko

Department of Aeronautics
Imperial College London
Exhibition road, London SW7 2AZ, UK
s.chernyshenko@imperial.ac.uk

Michael Leschziner

Department of Aeronautics
Imperial College London
Exhibition road, London SW7 2AZ, UK
mike.lechziner@imperial.ac.uk

ABSTRACT

Fully-developed turbulent flow in channels with oblique wavy walls is analysed, from a drag-reduction perspective, by means of Direct Numerical Simulations (DNS). The wavy geometry is chosen to emulate the shear strain produced by a Spatial Stokes Layer (SSL) generated by oscillatory wall motion. As the cost of performing a parametric optimisation is prohibitive, an alternate solution is presented, based on a linear model of a perturbed plane-channel flow, using a turbulent viscosity. Flow properties and levels of drag reduction or increase are reported for various configurations.

INTRODUCTION

As civilian aircraft manufacturers strive towards greener and more cost-efficient aviation, reducing turbulence-induced drag is a major target, as it accounts for about 50% of the total drag in cruise conditions. Motivated by the fact that even small drag reductions yield significant fuel savings, researchers have actively sought ways of controlling turbulence in order to reduce the drag. Amongst a range of techniques developed over the past few decades, imparting a spanwise oscillatory wall motion was first shown by Jung *et al.* (1992) to yield a significant reduction in streamwise wall friction. This original method of streamwise-homogeneous spanwise forcing was generalized by Quadrio (2011) to travelling waves, wherein the wall velocity is also space-dependent: $W(x,t) = A\sin(2\pi/\lambda_x x - \omega t)$. Although this control technique proved, by computations, to be very effective at reducing the viscous drag, practical applications are severely hindered by the absence of an efficient and maintainable actuation device. So far, in terms of net energy savings taking the total power supplied to the actuator into account, the most efficient laboratory implementation of the oscillating-wall technique has been achieved by Gatti *et al.* (2015). However, only small forcing amplitudes were permitted by the actuator, thus yielding a gross drag-reduction level of only 2.4% for the best case, for which the power of the actuation devices surpassed this reduction, thus rendering the overall net energy balance negative.

In the case of standing waves $\omega = 0$, i.e. for steady forcing, Viotti *et al.* (2009) showed that the so-called Spatial Stokes Layer (SSL), resulting from the in-plane wall motion, was more efficient than purely oscillating walls, yielding greater net energy savings, if a perfect actuator was assumed. Building on the steady nature of this actuation, Chernyshenko (2013) suggested the use of a skewed wavy wall in order to emulate a SSL. Forced obliquely across the wavy wall, the flow undergoes a spatially-varying pres-

sure gradient, thereby giving rise to a spatially varying spanwise motion without any active actuation. The key premise of the analysis in Chernyshenko (2013), based on earlier work on wall-actuated control, is that the drag reduction is not a consequence of the spanwise velocity itself, $W_{SSL}(x) = A_{SSL}\sin(2\pi/\lambda_x x)$, but rather of the associated shear strain $\partial W_{SSL}/\partial y$. Using semi-empirical estimates, Chernyshenko (2013) determined that a wave of the form $h_w(x,z) = A_w \sin(2\pi/\lambda_x x + 2\pi/\lambda_z z)$, with $\lambda_x^+ = 1520$, at an angle of approximately $52°$, was a good candidate for achieving a worthwhile level of drag reduction. The relatively long wavelength and the passive nature of the device promise, if proven effective, to be a significant step towards practical realisations of turbulent drag reduction. The main goal of the work presented herein is to seek a wavy-wall configuration capable of reducing the total drag, when compared to that experienced on a flat plate.

The structure of this paper is divided into two parts: first, direct numerical simulations of the flow are presented and the total drag is quantified, and second, a semi-empirical model is formulated in order to seek a configuration with maximum drag reduction.

NUMERICAL EXPERIMENTS
Description of the simulations

Direct numerical simulations have been performed using the code STREAMLES, a finite-volume, second-order accurate incompressible Navier-Stokes solver. The computed configuration is a wavy channel, of half-height h, with both solid walls undulating in phase. An integer number of waves is accommodated in the domain, allowing spanwise periodicity to be retained in both wall-parallel directions. The parameters defining the wavy surface are shown in fig. 1. In what follows, a flow configuration will be defined as a set of values (A_w, λ, θ).

A total of eight simulations, at $Re_\tau \approx 360$, are presented below:

- W0 corresponds to the configuration arising from the approach of Chernyshenko (2013);
- simulations W1A* (W1A1 to W1A4) correspond to the same wave as W0, but at a different angle, and
- W2A* features a smaller wavelength and is at the same angle as W1A*.

Evaluation of the drag

The steady spanwise forcing, caused by the presence of the wavy boundaries, is expected to reduce the friction drag if the em-
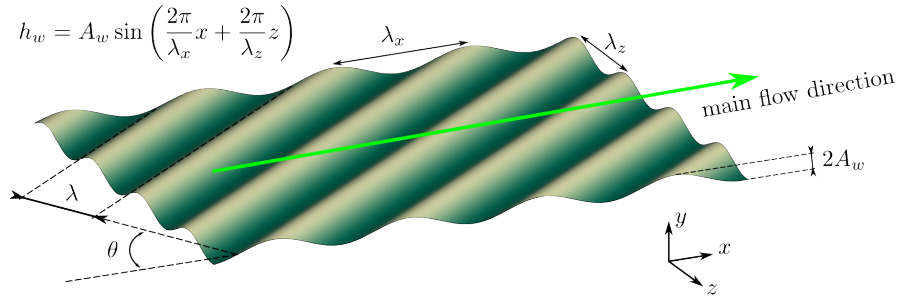
Figure 1. Parameters of the flow configuration, which can equivalently be defined by (A_w, θ, λ) or $(A_w, \lambda_x, \lambda_z)$; λ_x and λ_z are, respectively, the streamwise- and spanwise-projected wavelengths of the wavy wall.

Table 1. Drag quantification for the simulations presented. Relative variations with respect to the drag level in the baseline flow are given: Friction Drag Reduction (FDR), Pressure Drag (PD), Total Drag (TD). Negative values of TD indicate drag reduction. Viscous units are based on the baseline friction velocity.

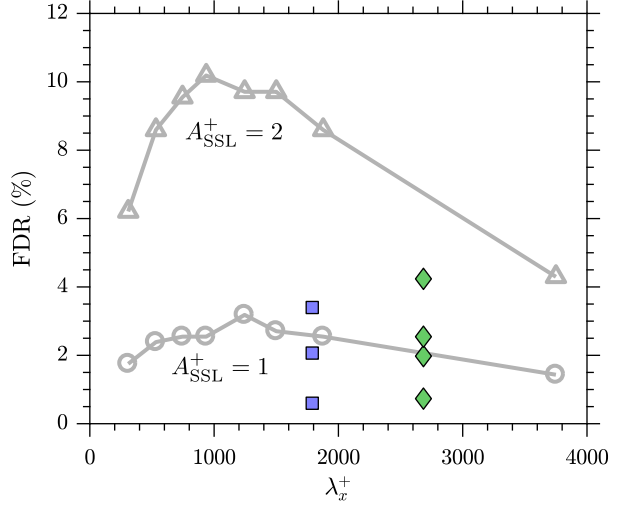|	λ^+	θ	A_w^+	FDR	PD	TD
W0	918	52°	18	4.8%	8.0%	+3.2%
W1A1	918	70°	11	0.7%	0.5%	-0.3%
W1A2	918	70°	18	2.0%	1.3%	-0.7%
W1A3	918	70°	22	2.6%	2.0%	-0.6%
W1A4	918	70°	32	4.2%	5.0%	+0.7%
W2A1	612	70°	7	0.6%	0.5%	-0.1%
W2A3	612	70°	14	2.1%	2.1%	-0.0%
W2A4	612	70°	22	3.4%	4.2%	+1.5%

Figure 2. Friction-drag reduction (FDR) from the baseline for SSL (gray symbols extracted from a digitised plot of Viotti *et al.* (2009), upper curve: $A_{\rm SSL}^+ = 2$; lower curve: $A_{\rm SSL}^+ = 1$) and for wavy wall; lozenges: W1A* ($\lambda^+ = 918$), squares: W2A* ($\lambda^+ = 612$).

ulation of a SSL is successful. Unlike in the SSL case, there is no power expended at the solid wavy wall, rather, the penalty for the generation of the drag-reducing spanwise motion is pressure drag. The net drag reduction / increase is thus obtained as the difference in total (skin-friction and pressure) drag of the wavy channel relative to the baseline plane channel. In order to reduce the impact of numerical errors on the quantification of the drag-reduction level, the computational grid for the baseline channel is chosen to be the same as that for the wavy channel, except for the vanishing amplitude $A_w = 0$. Because the absolute value of the drag depends slightly on the numerical resolution, despite the use of a grid finer than usually adopted for channel-flow DNS (the finest resolution is $\Delta x^+ = \Delta z^+ < 2$), the effect on the modest drag-reduction/increase levels is observed to be non-negligible, and the results therefore have to be treated with care. In each case, the drag is obtained by integration of the pressure and wall shear stress over the two wavy surfaces. This is then verified by comparison with the total pressure gradient across the streamwise computational box.

Table 1 gathers the main results. These indicate that a drag-reduction level of almost 1% could be attained for certain combinations of parameters. Interestingly, it is observed that the configuration W0, indicated as being the best by the analysis of Chernyshenko (2013), actually results in drag increase for $\theta = 52°$, but the same geometry at $\theta = 70°$ (W1A2) yields a positive drag reduction.

Comparison with SSL

The wavy boundary creates a spatially-periodic spanwise pressure gradient that gives rise to a spanwise motion. The waves also generate a streamwise pressure gradient, causing acceleration of the fluid on the windward side of the wave and deceleration on the leeward side. The amplitude of the spanwise motion generated by the wavy wall is smaller than the change in the streamwise velocity. This results in a fundamental difference between wavy walls and SSL, but despite the absence of a one-to-one correspondence between the wavy-wall configuration (A_w, λ, θ) and an ideally equivalent SSL configuration $(A_{\rm SSL}, \lambda_x = \lambda/\cos\theta)$, it is observed that the shear-strain field for streamwise-wave-slope values of $A_w/\lambda_x \approx 0.012$ and $A_w/\lambda_x \approx 0.007$ approximately emulates SSL's at same λ_x and respective forcing amplitudes $A_{\rm SSL}^+ = 1$ and $A_{\rm SSL}^+ = 2$.

The friction-drag-reduction level of each configuration is compared to that of the SSL case in fig. 2. For $A_{\rm SSL} = 1$, the friction reduction obtained in the SSL case is in line with what is obtained with a wavy wall with a streamwise wave slope of about 0.007. However, at the largest wave slope, despite the phase variations of the spanwise shear strain being of the same order as that of the SSL, a much lower level of friction-drag reduction is achieved. Thus, the emulation of the effect of the Stokes layer is not as successful for larger wave heights.

As a conclusion on the observations that can be made from the DNS results, it is observed that some wavy-wall channel configurations may have a slightly lower drag than the plane-channel baseline. Also, the spanwise shear-strain is approximately comparable to that of a Stokes layer, thus supporting the assumption that the friction is reduced by a similar mechanism. For small wave heights, the friction reduction achieved by the wavy wall is comparable to that achieved by the SSL for a similar spanwise shear-strain amplitude. However, this is not the case for larger wave heights for which the friction reduction is much lower than that of the SSL, thus indicating the presence of a different mechanism, which would explain why the configuration W0 is not effective.

SEMI-EMPIRICAL MODEL

A simplified model of the wavy-channel flow is formulated by assuming a gentle sinusoidal perturbation of a plane channel. A geometric wavy perturbation, as shown in fig. 1, is applied at both walls, so that the distance between the walls is constant everywhere and equal to $2h$. Reynolds-averaged Navier-Stokes equations, incorporating an eddy-viscosity model, are linearized in a transformed coordinate system and solved by a direct matrix inversion.

With time-averaging denoted by an overbar, and the Kronecker delta function identified by δ_{ij}, the modelled equations, with velocity and pressure written in wall units, are

$$\begin{cases} \dfrac{\partial}{\partial x_j}\left[\bar{u}_i\bar{u}_j+\bar{p}\,\delta_{ij}-\dfrac{1+\nu_t}{Re_\tau}\left(\dfrac{\partial\bar{u}_i}{\partial x_j}+\dfrac{\partial\bar{u}_j}{\partial x_i}\right)\right]=0 \\[2mm] \dfrac{\partial\bar{u}_i}{\partial x_i}=0 \end{cases} \quad (1)$$

The linear perturbation of the plane-channel flow considered is

$$\bar{q}(x,y,z)=q_0+A_w\Re(\hat{q}(\eta)\exp[\mathrm{i}(k_x x+k_z z)])=q_0+\tilde{q}, \quad (2)$$

where $\Re$ denotes the real part, $\eta=(y-h_w)/h$ the wall-normal location, ranging from -1 at the lower wall, to 1 at the upper wall, and $\hat{q}=[\hat{u},\hat{v},\hat{w},\hat{p}]^T$ is the solution vector of the linear system. The phase variations, i.e. free of the streamwise- and spanwise-integrated mean contributions, are $\tilde{q}$; $q_0=[U(\eta),0,0,-P_x x]^T$, with $P_x=1$ the driving pressure gradient normalised by the friction velocity, and $U(\eta)$ is the plane-channel velocity profile obtained from the RANS equations for $A_w=0$ (similar to equation (2.1c) in Reynolds & Tiederman (1967)):

$$1+\frac{\mathrm{d}}{\mathrm{d}\eta}\left[\frac{1+\nu_t}{Re_\tau}\frac{\mathrm{d}U}{\mathrm{d}\eta}\right]=0. \quad (3)$$

The eddy viscosity, shown in fig. 3, normalised by the fluid viscosity, is a function of the wall-normal coordinate only, and is defined using two constants c_1 and c_2 as in Moarref & Jovanović (2012):

$$\nu_t=\frac{1}{2}\left(\sqrt{1+\left\{\frac{c_2}{3}Re_\tau\left[1-\eta^2\right]\left[1+2\eta^2\right]\left[1-\exp\left(-Re_\tau\frac{1-|\eta|}{c_1}\right)\right]\right\}^2}-1\right). \quad (4)$$

Next, the expression in equation eq. (2) is inserted into the RANS equations eq. (1) and only the first-order terms are retained. With the operator M defined as

$$M=\mathrm{i}k_x U-\frac{1+\nu_t}{Re_\tau}\left[\left(\frac{\mathrm{d}^2}{\mathrm{d}\eta^2}-\|k\|^2\right)+\frac{\nu_t'}{1+\nu_t}\frac{\mathrm{d}}{\mathrm{d}\eta}\right], \quad (5)$$
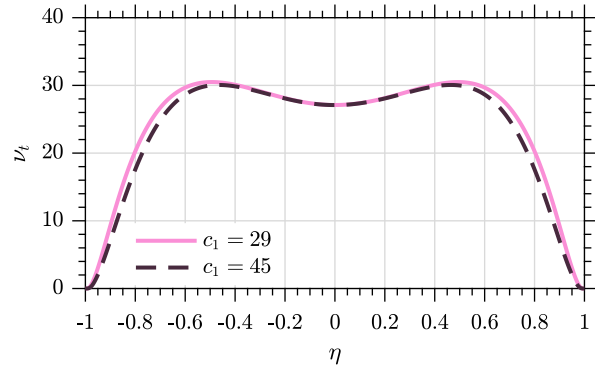

Figure 3. Eddy-viscosity as defined in eq. (4), for $c_1\in\{29,45\}$ and $c_2=0.46$; continuous line: $c_1=29$, dashed line: $c_1=45$.

where primes denote differentiation with respect to η, and $k=[k_x,k_z]^T$, the linearised set of equations can be written in matrix form as

$$\begin{bmatrix} \mathrm{i}k_x & \dfrac{\mathrm{d}}{\mathrm{d}\eta} & \mathrm{i}k_z & 0 \\[2mm] M & U'-\mathrm{i}k_x\dfrac{\nu_t'}{Re_\tau} & 0 & \mathrm{i}k_x \\[2mm] 0 & M & 0 & \dfrac{\mathrm{d}}{\mathrm{d}\eta} \\[2mm] 0 & -\mathrm{i}k_z\dfrac{\nu_t'}{Re_\tau} & M & \mathrm{i}k_z \end{bmatrix} \begin{bmatrix}\hat{u}\\[2mm]\hat{v}\\[2mm]\hat{w}\\[2mm]\hat{p}\end{bmatrix} = \begin{bmatrix} -\mathrm{i}k_x U' \\[2mm] k_x U U'-\mathrm{i}U'\|k\|^2\dfrac{1+\nu_t}{Re_\tau} \\[2mm] 0 \\[2mm] 0 \end{bmatrix}, \quad (6)$$

where the first three rows correspond to the momentum equations and the last one to the continuity equation. The system eq. (6) is inverted by direct matrix inversion with a one-dimensional second-order finite-difference discretisation used for the derivatives.

Model-predicted profiles of the velocity components and pressure at various phases are shown in fig. 4. Fair agreement is observed with DNS at $Re_\tau\approx 360$ using a different eddy viscosity for the prediction of the streamwise and spanwise velocities ($c_1=45,c_2=0.46$), from that of the wall-normal velocity and pressure ($c_1=29,c_2=0.46$).

Next, the linear model is used to find an estimate of the optimal set of parameters. An important feature of the present approach is that the linear model is not used to predict the total drag level directly. Instead, the drag variation (relative to the baseline drag) is split into pressure and friction contributions, each one being evaluated separately, as described below.

The friction drag is estimated indirectly by assuming that the reduction in friction is similar to that of a SSL at the same λ_x^+, and $A_{\mathrm{SSL}}^+=1$. An estimate of this value is given by a fit, denoted $\mathrm{FDR_{SSL}}(\lambda_x)$, of the data given in Viotti $et\ al.$ (2009) at $A_{\mathrm{SSL}}^+=1$, as shown in fig. 5. The latter depend on λ_x only, and they are rescaled to account for the higher Reynolds number, viz. $Re_\tau=360$ instead of 200, assuming that the drag-reduction level achieved by the SSL degrades with $Re_\tau^{-0.2}$, yielding the final expression for the friction-drag reduction (FDR):

$$\mathrm{FDR}=\mathrm{FDR_{SSL}}(\lambda_x)\left(\frac{Re_\tau}{200}\right)^{-0.2}. \quad (7)$$

The pressure drag is estimated by integration of the pressure along the wave. The relative variation from the baseline drag for
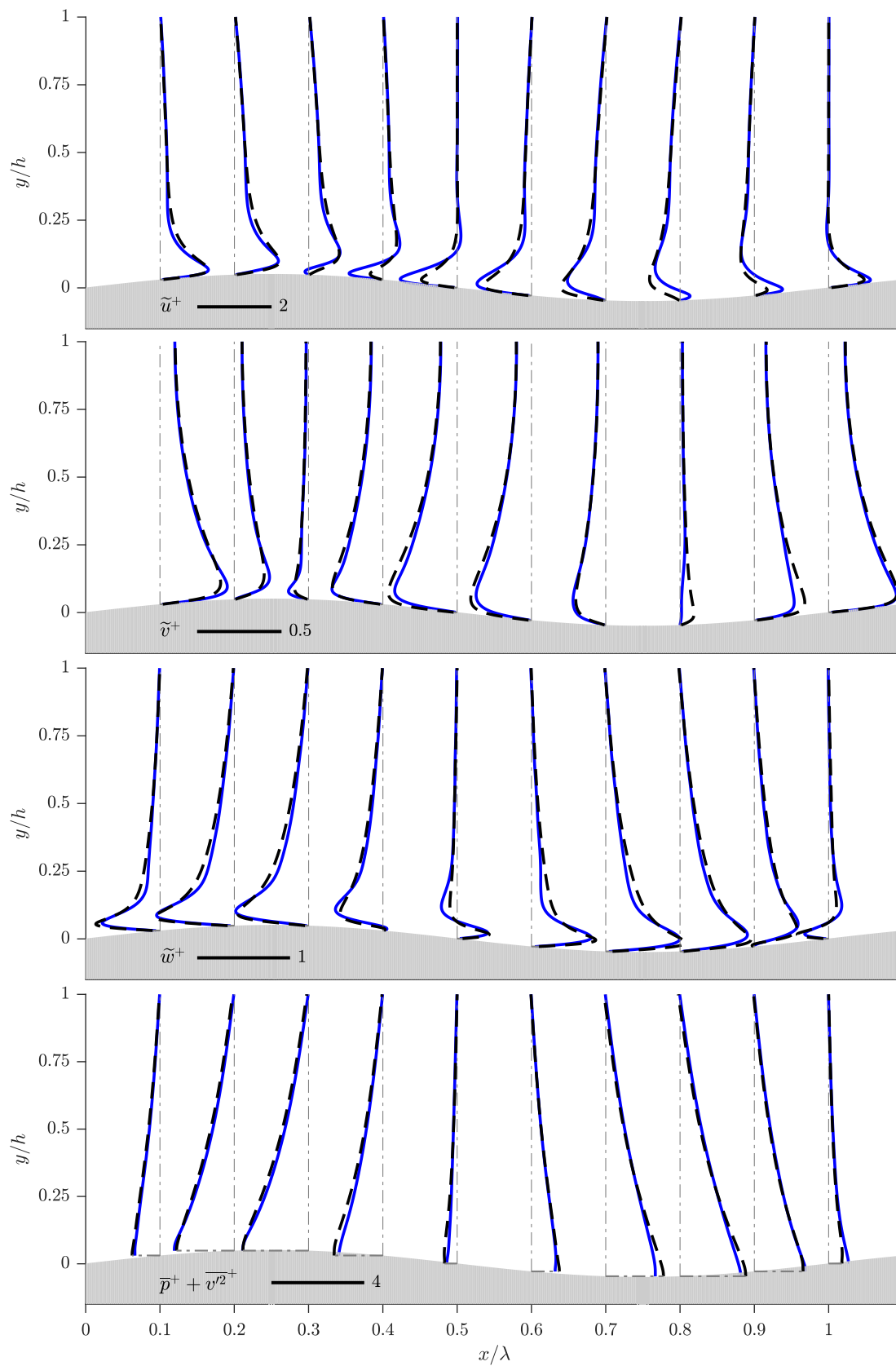
Figure 4. Comparison of the phase variations of the velocity components and pressure fields from the linear solver (dashed black line) and the DNS W1A2 (continuous blue line). Predictions for the streamwise and spanwise velocities are made with a different eddy viscosity ($c_1 = 45$) than that used for the prediction of the wall-normal velocity and pressure ($c_1 = 29$).
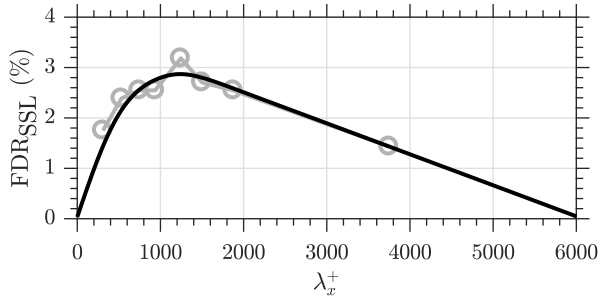
Figure 5. Curve fit to friction-drag reduction at $Re_\tau = 200$, used to estimate the equivalent drag reduction for the wavy-wall configuration (eq. (7)). Gray circles: data from Viotti *et al.* (2009), black line: fit of the numerical data used in the model.
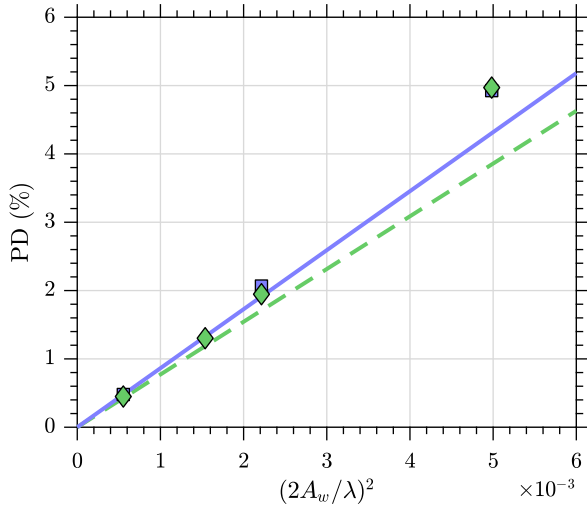

Figure 6. Pressure drag obtained from the linear model (lines), and from DNS (symbols); lozenges and dashed line: $\lambda^+ = 918$, squares and continuous line: $\lambda^+ = 612$.

the pressure drag becomes after integration:

$$\text{PD} = \frac{\pi}{\lambda_x} \Re\left[\hat{p}(-1)\right] A_w^2. \qquad (8)$$

The pressure drag calculated from the above equation is compared to the value obtained from DNS in fig. 6. For small wave slopes $(2A_w/\lambda < 0.05)$, the prediction of the pressure drag agrees within less than 0.2% of the baseline drag.

In order to estimate the optimum parameter combination, the parameter plane (θ, λ) is covered by a set of discrete combinations. For each combination, the required height of the wavy wall A_w is estimated, so that the maximum value of the spanwise velocity is constant, equal to $W_{\max}^+ = 0.85$, this value is close to that of the configuration W1A2, and yields a shear-strain field approximately similar to that of a laminar SSL with $A_{SSL}^+ = 1$. The drag contributions are estimated from eqs. (7) and (8). Fig. 7 shows the resulting map of the overall drag reduction, which presents an optimum close to $(\theta, \lambda^+) = (70°, 700)$, of about 0.8%. The implications of the semi-empirical results are twofold: first, the maximum drag-reduction level estimated is not large for such a small amplitude of actuation, and second, the trend is not consistent with the DNS results. Indeed, in table 1, for the two wavelengths $\lambda^+ = 918$ and $\lambda^+ = 612$, simulations W1A2 and W2A3 feature a spanwise shear-strain com-

parable to that of a SSL at $A_{SSL}^+ = 1$, but, whilst the drag reduction in W1A2 is of 0.7%, i.e. close to the semi-empirical prediction, it is about null for W2A3, contradicting the prediction of 0.8%. As shown in fig. 7, the achievable magnitude of drag reduction by a wavy wall, as predicted by the semi-empirical model, is quite small. In this respect, this is a conclusion similar to that obtained with a different semi-empirical model in Chernyshenko (2013).
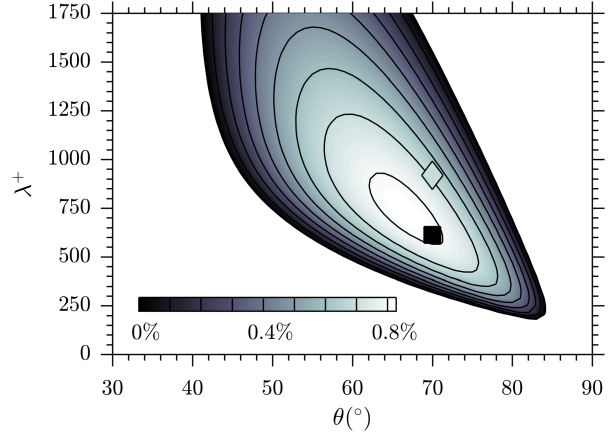

Figure 7. Estimation of the total drag reduction $\text{DR} = \text{FDR} - \text{PD}$ (in percent) using the semi-empirical model, assuming the wavy wall emulates a SSL of forcing amplitude $A_{SSL}^+ \approx 1$; symbols: DNS data (W1A2 and W2A3) coloured by the drag-reduction level.

CONCLUSIONS

Channel flow with oblique wavy walls, proposed as a means of emulating the drag reduction induced by a wall-actuated Stokes layer, was investigated by a combination of DNS and a semi-empirical model of the linearized Reynolds-averaged Navier-Stokes equations with prescribed eddy viscosity. A few promising flow configurations were selected and simulated at very high resolution. Such simulations are significantly more challenging than usual DNS of plane channels with actively induced Stokes layers – which feature much higher drag-reduction levels – consequently requiring substantially larger computational resources in order to reach sufficient accuracy that allows a fair estimation of drag-reduction levels that arise as a difference between friction-drag decrease and pressure-drag increase. The semi-empirical model was formulated in order to guide DNS studies towards parameter combinations that yield low-drag levels. The present analysis is adopted as an alternative to a formal shape optimisation, which was not tractable within the resources available. The model is able to reproduce the main features of the flow, and yields a good estimate of the pressure drag for small wave slopes. However, the analogy between the wavy wall and the SSL is tenuous, the wavy wall being less effective at reducing the friction. For small wave amplitudes, the behaviour is fairly close to that of the SSL, and this was exploited to derive a drag-reduction map for the wavy wall based on the properties of a SSL at a forcing amplitude of $A_{SSL}^+ = 1$. Regardless of the accuracy of the semi-empirical models, they suggest, along with the DNS results, that the optimum configuration is unlikely to yield maximum net drag reduction in excess of about 1%.

REFERENCES

Chernyshenko, S. 2013 Drag reduction by a solid wall emulating spanwise oscillations. Part 1. *ArXiv e-prints* **[physics.flu-dyn]** (arXiv:1304.4638).

Gatti, D., Güttler, A., Frohnapfel, B. & Tropea, C. 2015 Experimental assessment of spanwise-oscillating dielectric electroactive surfaces for turbulent drag reduction in an air channel flow. *Experiments in Fluids* **56** (5), 1–15.

Jung, W. J., Mangiavacchi, N. & Akhavan, R. 1992 Suppression of turbulence in wall-bounded flows by high-frequency spanwise oscillations. *Phys. Fluids* **4** (8), 1605–1607.

Moarref, R. & Jovanović, M. R. 2012 Model-based design of tranverse wall oscillations for turbulent drag reduction. *J. Fluid Mech.* **707**, 205–240.

Quadrio, M. 2011 Drag reduction in turbulent boundary layers by in-plane wall motion. *Philosophical Transactions of the Royal Society A* **369** (1940), 1428–1442.

Reynolds, W. C. & Tiederman, W. G. 1967 Stability of turbulent channel flow, with application to Malkus's theory. *J. Fluid Mech.* **27** (2), 253–272.

Viotti, C., Quadrio, M. & Luchini, P. 2009 Streamwise oscillation of spanwise velocity at the wall of a channel for turbulent drag reduction. *Phys. Fluids* **21** (115109).